Applied Physics Letters

# The interplay of intra- and inter-layer interactions in bending rigidity of ultrathin 2D materials

Cite as: Appl. Phys. Lett. **122**, 153101 (2023); https://doi.org/10.1063/5.0146065
Submitted: 09 February 2023 • Accepted: 28 March 2023 • Published Online: 11 April 2023

Yingchun Jiang, Srividhya Sridhar, Zihan Liu, et al.









AIP Publishing

Applied Physics Letters ARTICLE scitation.org/journal/apl

# The interplay of intra- and inter-layer interactions in bending rigidity of ultrathin 2D materials

Cite as: Appl. Phys. Lett. **122**, 153101 (2023); doi: 10.1063/5.0146065
Submitted: 9 February 2023 · Accepted: 28 March 2023 ·
Published Online: 11 April 2023



Yingchun Jiang,[1] Srividhya Sridhar,[2] Zihan Liu,[1] Dingli Wang,[1] Huimin Zhou,[3] Jia Deng,[3] Huck Beng Chew,[2,a)] and Changhong Ke[1,4,a)]

## AFFILIATIONS

[1]Department of Mechanical Engineering, State University of New York at Binghamton, Binghamton, New York 13902, USA
[2]Department of Aerospace Engineering, University of Illinois at Urbana-Champaign, Urbana, Illinois 61801, USA
[3]Department of Systems Science and Industrial Engineering, State University of New York at Binghamton, Binghamton, New York 13902, USA
[4]Materials Science and Engineering Program, State University of New York at Binghamton, Binghamton, New York 13902, USA

[a)]**Authors to whom correspondence should be addressed:** hbchew@illinois.edu and cke@binghamton.edu

## ABSTRACT

Continuum mechanics break down in bending stiffness calculations of mono- and few-layered two-dimensional (2D) van der Waals crystal sheets, because their layered atomistic structures are uniquely characterized by strong in-plane bonding coupled with weak interlayer interactions. Here, we elucidate how the bending rigidities of pristine mono- and few-layered molybdenum disulfide ($MoS_2$), graphene, and hexagonal boron nitride (hBN) are governed by their structural geometry and intra- and inter-layer bonding interactions. Atomic force microscopy experiments on the self-folded conformations of these 2D materials on flat substrates show that the bending rigidity of $MoS_2$ significantly exceeds those of graphene or hBN of comparable layers, despite its much lower tensile modulus. Even on a per-thickness basis, $MoS_2$ is found to possess similar bending stiffness to hBN and is much stiffer than graphene. Density functional theory calculations suggest that this high bending rigidity of $MoS_2$ is due to its large interlayer thickness and strong interlayer shear, which prevail over its weak in-plane bonding.



The fundamental mechanical properties of mono- and few-layered two-dimensional (2D) van der Waals crystals, such as graphene, molybdenum disulfide ($MoS_2$), and hexagonal boron nitride (hBN), are of great importance to the pursuit of a variety of their applications, such as electronics, composites, and sensors.[1,2] In particular, bending/flexural rigidity (stiffness) is a key parameter of 2D materials for applications in flexible electronic devices[3] and complex three-dimensional structures.[4] The bending rigidities of these layered 2D crystals differ from those of traditional solids because of their layered atomistic structures, strong in-plane bonding,[5,6] and weak interlayer interactions,[7,8] where continuum mechanics theory breaks down. In classical mechanics of materials, the bending stiffness of a fully bonded laminated plate is a cubic function of its thickness (or the number of laminates), but follows a linear function if the laminates are free to slide without friction. In comparison, recent studies show a square function relationship for the bending stiffness of few-layer graphene,[9] suggesting possibility of interlayer sliding with friction. Unlike the tensile modulus that is solely governed by in-plane bonding strength and interlayer thickness, the bending rigidity of layered 2D materials is also substantially influenced by interlayer adhesion and shear.[9–14] The weak van der Waals interactions that hold the stacked 2D sheets together result in low interlayer shear resistance and, thus, permit relative sliding between neighboring layers, which substantially lowers their bending rigidity.

To date, studies primarily focus on the bending rigidity of graphene and hBN,[9,10,15–20] with comparatively fewer reports on molybdenum disulfide ($MoS_2$).[16,21–24] In particular, experimental data for ultrathin (i.e., mono- or few-layer) $MoS_2$ remain scarce in the literature,[23,24] and the layer-number dependence of the bending stiffness of ultrathin $MoS_2$ remains elusive. $MoS_2$ is a 2D semiconductive transition metal dichalcogenide (TMD) material that is promising for many electronics applications.[25] $MoS_2$ reportedly possesses a Young's modulus of ~330 GPa,[26] which is much lower than graphene [~1 TPa (Ref. 6)] or hBN [~870 GPa (Ref. 5)]. In contrast to the flat in-plane hexagonal bonding network in both graphene and hBN, individual $MoS_2$ sheets possess a tertiary atomic structure in which single layer of Mo atoms is sandwiched between two layers of S atoms; these vertically stacked, covalently bonded S–Mo–S layers interact with neighboring

layers by van der Waals interactions. The interlayer thickness of $MoS_2$ is ~0.615 nm,[27] as compared to ~0.34 nm for both graphene and hBN.[28] The bending stiffness of $MoS_2$ and its comparison with those of graphene and hBN with comparable number of layers will provide insights on the interplay between intra- and inter-layer interactions in governing the bending rigidity of ultrathin 2D materials. In this Letter, we quantify the intrinsic bending stiffness of pristine mono- and few-layered $MoS_2$ flakes by measuring their self-folded configurations on flat silicon dioxide substrates [as illustrated in Fig. 1(a)] using atomic force microscopy (AFM), and comparing with those for graphene and hBN. Insights into the roles of interlayer adhesion and shear on the bending rigidities of $MoS_2$ vs graphene and hBN are obtained from density functional theory (DFT) calculations.

Mono- and few-layer $MoS_2$ flakes employed in this study were prepared by first mechanically exfoliating bulk $MoS_2$ crystals (SPI supplies). These flakes were then transferred onto clean silicon substrates with a 285-nm $SiO_2$ layer grown on top, using scotch tapes as the transfer media. Some of the transferred $MoS_2$ flakes were found to stay in a self-folded conformation, and the folding likely occurred during the exfoliation and/or transfer processes. It is noted that thermal annealing was intentionally avoided to preserve the pristine folding morphology of $MoS_2$ (see Fig. S1 in the supplementary material). The thickness and the number of layers of $MoS_2$ flakes were identified by optical contrast, Raman spectroscopy (see Fig. S2 in the supplementary material) and AFM imaging. In the substrate-bounded folding configuration, the number of layers in a $MoS_2$ flake (or its actual thickness) can be accurately characterized by measuring the step height of the folded segment over the flat (unfolded) segment in the adhered region.[29] Among 98 characterized $MoS_2$ specimens, 34 flakes with clean surface and uniform folding edge were identified to be 1–5 layers and are used in the bending stiffness analysis. Figures 1(b)–1(d) show representative AFM images of self-folded monolayer (1L), bilayer (2L), and trilayer (3L) $MoS_2$ on silicon oxide substrates and the corresponding line profiles over folding edges, which have hump heights of 0.61, 1.35, and 2.15 nm, respectively. Figure 1(e) shows that the hump height of self-folded $MoS_2$ flakes linearly increases with the number of layers.

We note that the self-folding conformation of a 2D sheet on a flat substrate results from a balance between the bending energy in the

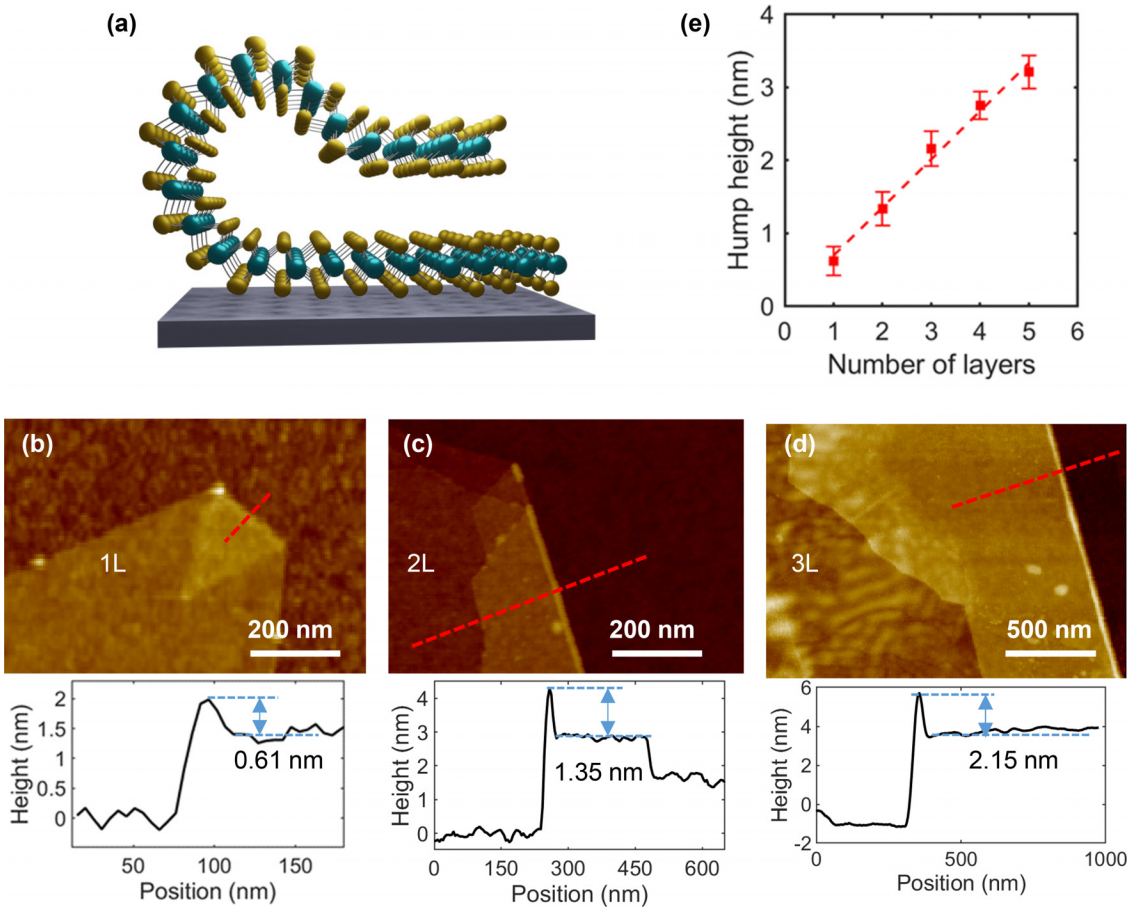


**FIG. 1.** Self-folding of single $MoS_2$ flake on a flat substrate. (a) Schematic of the self-folding monolayer $MoS_2$ on a $SiO_2$/Si substrate; (b)–(d) representative AFM images of self-folded 1L to 3L flakes and the respective line profiles of the flake height along the marked red dashed lines; and (e) plot of the hump height of the folding edge with respect to the number of layers based on measurements of 34 self-folded $MoS_2$ flakes that were identified to be 1–5L. The error bars in the plot are the standard deviations based on at least four independent AFM height measurements.

folded segment and the adhesion interactions between the 2D segments in the adhered region as well as between the folded segment and the substrate. Therefore, the hump height of the folding profile is an indicator of the magnitude of the bending stiffness of 2D sheets. Using a nonlinear continuum mechanics model, we calculate the bending stiffness of 1–5L $MoS_2$ flakes directly from the measured hump heights. Here, the 2D sheet is considered as an inextensible elastic sheet and its deformation is governed by pure bending,[30] thus neglecting the stretching effect. The self-folding of one 2D sheet on a flat substrate initiates with a partial delamination of the sheet from the substrate, followed by its subsequent folding to adhere to its unfolded segment. The deformational profile of the 2D sheet, as schematically shown in Fig. 2(a) (blue curves: outer surfaces; black curve: mid-plane), can be divided into three segments: (i) a curved region from points A to E with point A as the heal front and point E as the delamination front; (ii) an overlapped (adhered) region with an equilibrium distance $d = N \times t$, where $N$ is the number of layers and $t$ is the interlayer thickness; and (iii) a flat contact region between the flake and the substrate. We adopt a Cartesian coordinate system with the $x$ axis defined along the symmetric plane of the overlapping region, and the y axis is taken through point A. Points B, C, D, and E represent the inflection point connecting the convex curve AB and the concave curve BC, the highest point of the folding conformation, the right most point, and the point where the folding meets the supporting substrate, respectively. The governing equation of the curved region is given as

$$D\left[\left(\frac{d\kappa}{ds}\right)^2 + \frac{\kappa^4}{4}\right] + C_1\kappa^4 + C_2 = 0, \quad (1)$$

where $D$ is the per-unit-length bending stiffness of the 2D sheet, $s$ is the natural coordinate along the deformation curve starting from point A, $\kappa$ is the bending curvature, and $C_1$ and $C_2$ are two integration constants that are determined from boundary conditions (see the supplementary material). The boundary conditions include the deformation curvatures at the delamination and heal fronts that are given as $\kappa_E = \sqrt{2G_{2D-Sub}/D}$ and $\kappa_A = \sqrt{2G_{2D-2D}/D}$, respectively, where $G_{2D-Sub}$ is the adhesion energy per unit area between the 2D sheet and the substrate and $G_{2D-2D}$ is the adhesion energy per unit area between two adhered 2D sheets. The binding energy for $MoS_2$ reportedly varies little with its number of layers and the experimental value $G_{2D-2D} = 0.55\ J/m^2$ from Ref. 31 is used in the calculation. The experimental value $G_{2D-Sub} = 0.17\ J/m^2$ from Ref. 32 is also adopted in the calculation.

Figure 2(b) shows the predicted deformation profiles at equilibrium of self-folded 1L to 5L $MoS_2$ sheets based on the measured mean hump height by solving Eq. (1). Figure 2(c) shows the calculated bending stiffness of 1L to 5L $MoS_2$ based on the measured hump heights

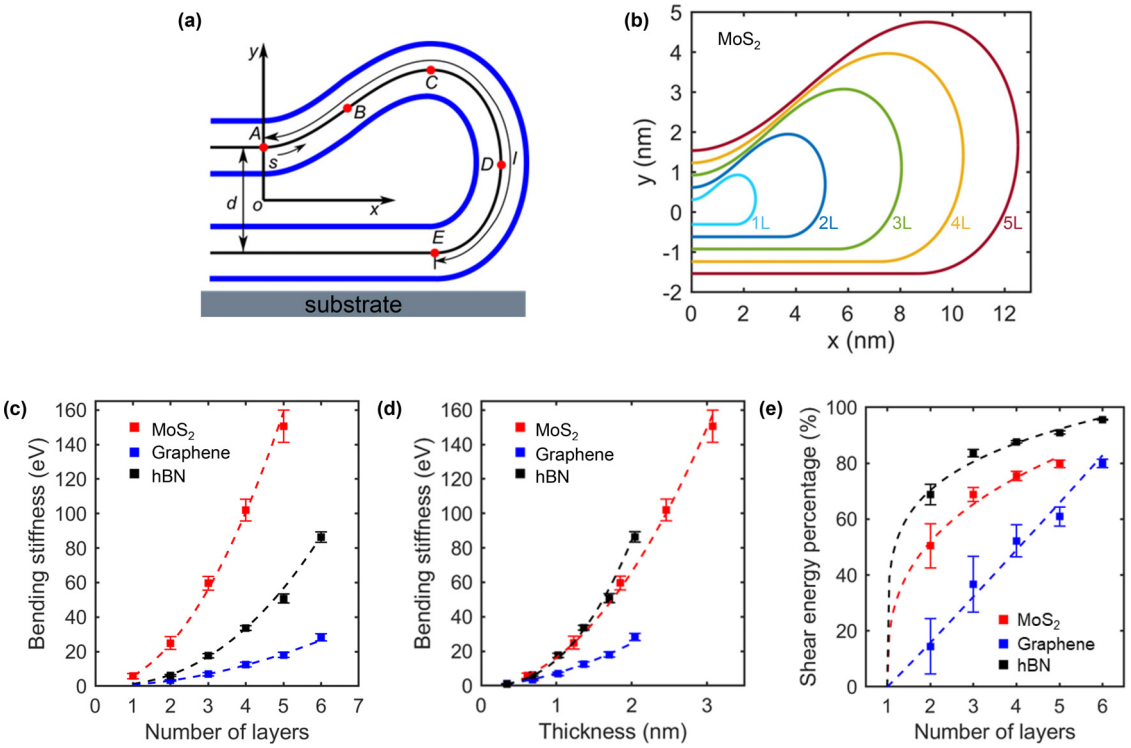


**FIG. 2.** (a) Continuum mechanics model of the self-folded 2D flake on a flat substrate. The two blue curves indicate two outer surfaces of the flake. The black curve indicates the middle-plane deformation profile. (b) The calculated middle-plane deformational profiles of self-folded 1L to 5L $MoS_2$ flakes. (c) and (d) The comparison of the bending stiffness of $MoS_2$, graphene, and hBN. (e) The comparison of the interlayer shear energy contribution to the overall bending energy of 2D sheets. The dashed lines are the respective power-function fitting curves. The bending stiffness values for graphene are reproduced from Ref. 9. The bending stiffness values for 1L and 2–6L hBN are reproduced from Refs. 20 and 10, respectively.

**TABLE I.** The comparison of the bending stiffness and interlayer shear contribution for mono- and few-layer $MoS_2$, graphene, and hBN. The bending stiffness values for graphene are reproduced from Ref. 9. The bending stiffness values for 1L and 2–6L hBN are reproduced from Refs. 20 and 10, respectively.

| | Bending stiffness (eV) | | | Interlayer shear energy contribution (%) | | |
|---|---|---|---|---|---|---|
| # of layers | $MoS_2$ | hBN | Graphene | $MoS_2$ | hBN | Graphene |
| 1 | 6.0 ± 1.5 | 0.95 | 1.3 | 0 | 0 | 0 |
| 2 | 25.1 ± 3.7 | 6.2 ± 0.6 | 3.4 ± 0.4 | 50.5 ± 7.9 | 68.8 ± 3.6 | 14.5 ± 9.9 |
| 3 | 57.9 ± 4.0 | 17.7 ± 1.2 | 6.9 ± 0.9 | 68.8 ± 2.4 | 83.7 ± 1.3 | 36.7 ± 10.0 |
| 4 | 102.3 ± 6.3 | 33.6 ± 1.4 | 12.5 ± 1.3 | 75.4 ± 1.7 | 87.7 ± 0.5 | 52.2 ± 5.7 |
| 5 | 150.8 ± 9.3 | 50.8 ± 2.6 | 18.1 ± 1.5 | 79.8 ± 1.3 | 90.9 ± 0.6 | 61.0 ± 3.4 |
| 6 | ⋯ | 86.3 ± 3.1 | 28.3 ± 2.1 | ⋯ | 95.6 ± 0.2 | 80.0 ± 1.5 |

[Fig. 1(e)], which is also listed in Table I. The bending stiffness of $MoS_2$ increases substantially with its number of layers ($N$), and the dependence follows a power-function given as $D = 15.7(N \times t)^{2.035}$ with an R-squared fitting value >0.99. The bending stiffness of monolayer $MoS_2$ $D_{1L} = 6.0 \pm 1.5$ eV is in excellent agreement with the predicted value (5.44–7.17 eV)[21] that is obtained based on the DFT-calculated elastic constants and is modestly lower than the theoretical values [9.61 eV (Ref. 22) and 9.8–13.4 eV (Ref. 21)] from molecular dynamics (MD) simulations or the experimental values (∼10.26–10.5 eV) that are derived based on transmission electron microscopy (TEM) imaging of folded $MoS_2$ structures.[23,24] The bending stiffness of monolayer $MoS_2$ is substantially higher than the reported theoretical values of both graphene (∼1.3 eV)[9] and hBN (0.95 eV).[20] Figure 2(c) also shows a comparison with the bending stiffness of 2–6L graphene[9] and hBN[10] sheets that were characterized using the same experimental and theoretical methodologies. Results show that the folded $MoS_2$ sheets consistently possess a much higher bending stiffness than graphene or hBN sheets with the same number of layers, despite $MoS_2$ possessing lower in-plane Young's modulus of ∼330 GPa (Ref. 26) vs ∼1 TPa for graphene[6] and ∼870 GPa for hBN.[5] Since the bending rigidity of monolayer 2D crystals originates entirely from the stretching and/or compression of chemical bonds and is free of any interlayer interactions, the high bending stiffness even for monolayer $MoS_2$ implies that the flake thickness has a prominent influence on its bending rigidity. Our DFT calculations (see the supplementary material) accounting for van der Waals interactions show that the relaxed graphene, hBN, and $MoS_2$ bilayers have average interlayer separation distances (i.e., layer thickness) of 3.2, 3.1, and 6.2 Å, respectively. The twofold thicker $MoS_2$ interlayer explains its higher bending stiffness when compared with graphene or hBN with the same number of layers [Fig. 2(c)]. In fact, the comparison of the bending stiffness vs the thickness of the 2D sheets in Fig. 2(d) shows that $MoS_2$ and hBN actually possess similar bending stiffness at the same thickness, and both are much stiffer than graphene. We attribute this increased bending stiffness of hBN and $MoS_2$ vs graphene to interlayer shear effects.

To quantify the influence of interlayer interaction on the bending rigidity of 2D materials, we calculate the contribution of the interlayer shear energy from bending-induced relative sliding in neighboring layers to the total bending energy of few-layer 2D crystals based on their measured bending stiffness. The total energy in the curved 2D sheet with a length of $l$ [Fig. 2(a)] $E_{tot} = \frac{D}{2}\int_0^l k^2 ds$ is considered to comprise two parts: (i) the pure bending energy stored in individual layers $E_b = \frac{D_{1L}}{2}\sum_{i=1}^{N}\int_0^l k_i^2 \mathrm{d}s$, which originates from in-plane bond stretching, and (ii) the interlayer shear energy $E_s = E_{tot} - E_b$, which represents the adhesion contribution across layers and is zero for monolayer 2D crystals. Here, the stretching of individual layers[14] is considered to be negligible based on the free slide boundary conditions at both ends of each layer. Figure 2(e) shows the interlayer shear contribution to the total bending energy ($= E_s/E_{tot}$) calculated for $MoS_2$, hBN, and graphene, all of which follow monotonically increasing power functions with the number of interlayers ($N - 1$). The interlayer shear energy for $MoS_2$ [∼50.5% (2L) to ∼79.8%(5L)] is higher than those for graphene [∼14.5% (2L) to ∼61.0% (5L)], but lower than those for hBN [∼68.8% (2L) to ∼90.9% (5L)]. For both $MoS_2$ and hBN, the contribution of the interlayer shear energy to the overall bending stiffness saturates with the increase in number of crystal layers, $N$. In contrast, the interlayer shear contribution linearly increases with $N$ for graphene. The results reveal that the interlayer shear significantly contributes to the bending stiffness (>50%) of bilayer $MoS_2$ and hBN, and as the number of layers increases, the interlayer shear gradually tapers to approach 100% contribution, implying that bending response is governed by interlayer shear at higher number of layers. On the contrary, for 2L graphene, the contribution of interlayer shear is small (<20%), implying that the bending stiffness mostly comes from in-plane stiffness. Thus, even though both $MoS_2$ and hBN have a lower in-plane stiffness as compared to graphene, much of their bending stiffness originates from the interfacial shear especially for few layer sheets. This implies that $MoS_2$ and hBN sheets possess substantially higher interfacial shear resistance than graphene—a finding which is later corroborated by our DFT calculations. When the number of layers increases beyond 6, the trend implies that the bending response is almost entirely dominated by interlayer shear, while in-plane stiffness no longer plays a substantial role.

To obtain further insights into the differing bending stiffness across the graphene, hBN, and $MoS_2$ interlayers, we perform DFT calculations to construct supercells of dual-layer graphene/hBN/$MoS_2$ (see the supplementary material). Figure 3 shows the potential energy landscapes for interlayer sliding between graphene/graphene, hBN/hBN, and $MoS_2$/$MoS_2$ sheets, respectively, obtained by iteratively displacing the top atomic sheet with respect to the bottom sheet along the two in-plane lattice vectors of each supercell, while allowing the atoms to relax in the vertical direction. Since the folding orientation of the 2D sheets in our experiments is random, the multilayer 2D sheets

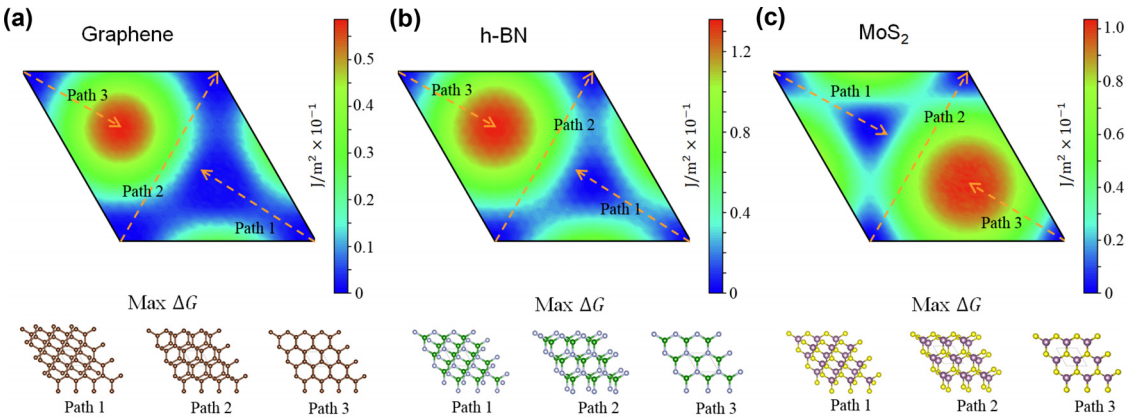


**FIG. 3.** Potential energy landscapes for interlayer sliding along bilayer graphene (a), hBN (b), and $MoS_2$ (c). Three potential sliding energy paths are denoted, along with the top-view of the atomic configuration at the sliding barriers along these paths. Atom colors: C (brown), B (green), N (white), Mo (purple), and S (yellow).

could fold along different crystal orientations. In view of this, we highlight three potential pathways for the sliding of the atomic sheets from one AB (minimum energy) stacking to another AB or BA stacking configuration for each 2D structure, and we include the top-view of the atomic configurations at the barrier energy (maximum ΔG) along each of these pathways. We trace in Fig. 4 the changes in the sliding potential energy along each of these pathways, where the peak barrier energies ΔG associated with these pathways can be interpreted as the range of sliding barrier energies applicable for different folding orientations. Our results show that the sliding barrier energy for both $MoS_2$ and hBN is very comparable along paths 1 and 2, but hBN has a distinctly higher barrier energy than $MoS_2$ along path 3 where we have an unstable AA stacking arrangement. Comparatively, the sliding barrier energies for graphene bilayers are consistently lower than those for hBN and $MoS_2$, which implies lower interfacial shear stiffness for the graphene bilayers. The comparable interlayer sliding barriers for both hBN and $MoS_2$ from our simulation results explain their similar bending stiffness when compared across multilayer 2D crystal sheets of the same thickness [Fig. 2(d)]. In contrast, the distinctly lower interlayer sliding barrier energies for graphene explain the significantly lower contribution of interlayer shear to its bending stiffness [Fig. 2(e)].

It is noted that the DFT calculations consider the lowest energy stacking configuration of the self-folded sheets, while the adhesion energy could be smaller when the folded sheets are stacked in the non-energy-minimum (non-AB) configurations, such as at locations of maximum ΔG along Paths 1 to 3 in Fig. 3. The variations in ΔG along the lower energy sliding paths 1 and 2, however, are significantly lower than the adhesion energies of 0.34, 0.42, and 0.23 $J/m^2$ for graphene, h-BN, and $MoS_2$, respectively, which we obtain by subtracting the energy of each relaxed bilayer from the total energy of the isolated 2D sheets. This suggests that varying folding orientations do not significantly change the self-adhesion energies of the respective sheets that were used in our earlier analytical calculations.

In summary, the bending rigidities of mono- and few-layered $MoS_2$ are characterized and compared with the respective values for graphene and hBN. The study reveals that $MoS_2$ possesses a substantially higher bending rigidity as compared to graphene or h-BN of comparable number of layers, which is attributed to its larger layer/interlayer thickness combined with its strong interlayer shear. The finding of high bending rigidity of ultrathin $MoS_2$ has important implications to its electronics applications. For example, ultrathin $MoS_2$ is less prone to out-of-plane structural instability, such as wrinkles and ripples that reportedly occur in 2D crystals[33,34] and

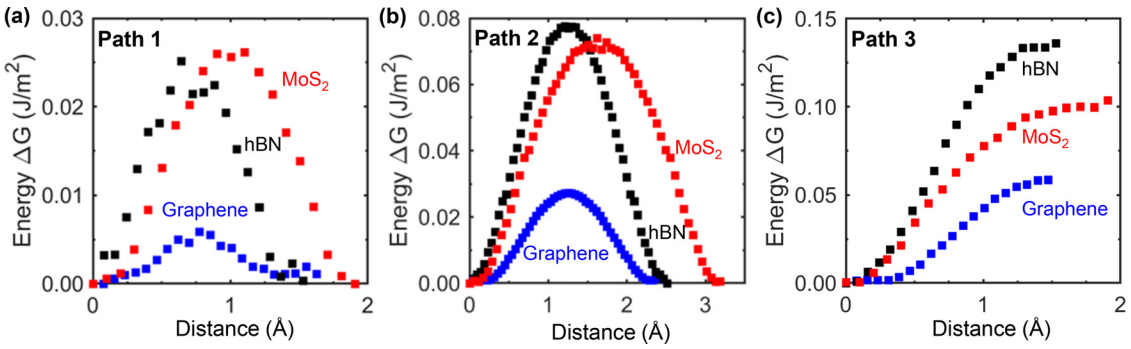


**FIG. 4.** Trace of potential energy for interlayer sliding along paths 1 to 3 in graphene, hBN, and $MoS_2$.

influence their electrical properties.[35–37] The superior bending rigidity enables ultrathin $MoS_2$ as a promising building block for the development of robust nanoelectronics and sensors.

See the supplementary material for the details about the experimental methods, the continuum model, and the computational method.

The authors acknowledge the support of the National Science Foundation under Grant Nos. CMMI 2009134, 2009684, and 2006127. The DFT calculations were performed using the computational time provided by Delta research computing project, which is supported by the National Science Foundation (Award No. OCI 2005572) and the State of Illinois. Delta is a joint effort of the University of Illinois at Urbana-Champaign and its National Center for Supercomputing Applications. The use of the Advanced Cyberinfrastructure Coordination Ecosystem: Services & Support (ACCESS), through allocation TG-MAT210031, is also gratefully acknowledged.

## AUTHOR DECLARATIONS

### Conflict of Interest

The authors have no conflicts to disclose.

### Author Contributions

Yingchun Jiang and Srividhya Sridhar contributed equally to this work.

**Yingchun Jiang:** Formal analysis (lead); Investigation (lead); Writing – review & editing (equal). **Srividhya Sridhar:** Formal analysis (lead); Investigation (lead); Writing – review & editing (equal). **Zihan Liu:** Formal analysis (equal); Investigation (equal); Writing – review & editing (equal). **Dingli Wang:** Formal analysis (equal); Investigation (equal); Writing – review & editing (equal). **Huimin Zhou:** Investigation (supporting); Writing – review & editing (equal). **Jia Deng:** Investigation (supporting); Writing – review & editing (equal). **Huck Beng Chew:** Conceptualization (equal); Supervision (equal); Writing – review & editing (equal). **Changhong Ke:** Conceptualization (equal); Supervision (equal); Writing – review & editing (equal).

## DATA AVAILABILITY

The data that support the findings of this study are available from the corresponding authors upon reasonable request.

## REFERENCES

[1]N. R. Glavin, R. Rao, V. Varshney, E. Bianco, A. Apte, A. Roy, E. Ringe, and P. M. Ajayan, "Emerging applications of elemental 2D materials," Adv. Mater. **32**(7), 1904302 (2020).
[2]J. H. Kim, J. H. Jeong, N. Kim, R. Joshi, and G.-H. Lee, "Mechanical properties of two-dimensional materials and their applications," J. Phys. D **52**(8), 083001 (2019).
[3]C. Xie and F. Yan, "Flexible photodetectors based on novel functional materials," Small **13**(43), 1701822 (2017).
[4]W. Lee, Y. Liu, Y. Lee, B. K. Sharma, S. M. Shinde, S. D. Kim, K. Nan, Z. Yan, M. Han, Y. Huang, Y. Zhang, J.-H. Ahn, and J. A. Rogers, "Two-dimensional materials in functional three-dimensional architectures with applications in photodetection and imaging," Nat. Commun. **9**(1), 1417 (2018).
[5]A. Falin, Q. Cai, E. J. G. Santos, D. Scullion, D. Qian, R. Zhang, Z. Yang, S. Huang, K. Watanabe, T. Taniguchi, M. R. Barnett, Y. Chen, R. S. Ruoff, and L. H. Li, "Mechanical properties of atomically thin boron nitride and the role of interlayer interactions," Nat. Commun. **8**, 15815 (2017).
[6]C. Lee, X. Wei, J. W. Kysar, and J. Hone, "Measurement of the elastic properties and intrinsic strength of monolayer graphene," Science **321**(5887), 385–388 (2008).
[7]X. Feng, S. Kwon, J. Y. Park, and M. Salmeron, "Superlubric sliding of graphene nanoflakes on graphene," ACS Nano **7**(2), 1718–1724 (2013).
[8]H. Li, J. Wang, S. Gao, Q. Chen, L. Peng, K. Liu, and X. Wei, "Superlubricity between $MoS_2$ monolayers," Adv. Mater. **29**(27), 1701474 (2017).
[9]X. Chen, C. Yi, and C. Ke, "Bending stiffness and interlayer shear modulus of few-layer graphene," Appl. Phys. Lett. **106**(10), 101907 (2015).
[10]W. Qu, S. Bagchi, X. Chen, H. B. Chew, and C. Ke, "Bending and interlayer shear moduli of ultrathin boron nitride nanosheet," J. Phys. D **52**(46), 465301 (2019).
[11]M. Rejhon, F. Lavini, A. Khosravi, M. Shestopalov, J. Kunc, E. Tosatti, and E. Riedo, "Relation between interfacial shear and friction force in 2D materials," Nat. Nanotechnol. **17**(12), 1280–1287 (2022).
[12]S. Peng and Y. Wei, "On the influence of interfacial properties to the bending rigidity of layered structures," J. Mech. Phys. Solids **92**, 278–296 (2016).
[13]X. Ma, L. Liu, Z. Zhang, and Y. Wei, "Bending stiffness of circular multilayer van der Waals material sheets," J. Appl. Mech. **89**(3), 031011 (2022).
[14]X. Chen, L. Zhang, Y. Zhao, X. Wang, and C. Ke, "Graphene folding on flat substrates," J. Appl. Phys. **116**(16), 164301 (2014).
[15]D.-B. Zhang, E. Akatyeva, and T. Dumitrică, "Bending ultrathin graphene at the margins of continuum mechanics," Phys. Rev. Lett. **106**(25), 255503 (2011).
[16]G. Wang, Z. Dai, J. Xiao, S. Feng, C. Weng, L. Liu, Z. Xu, R. Huang, and Z. Zhang, "Bending of multilayer van der Waals materials," Phys. Rev. Lett. **123**(11), 116101 (2019).
[17]E. Han, J. Yu, E. Annevelink, J. Son, D. A. Kang, K. Watanabe, T. Taniguchi, E. Ertekin, P. Y. Huang, and A. M. van der Zande, "Ultrasoft slip-mediated bending in few-layer graphene," Nat. Mater. **19**(3), 305–309 (2020).
[18]X. Ma, L. Liu, Z. Zhang, and Y. Wei, "A method to determine the geometry-dependent bending stiffness of multilayer graphene sheets," J. Appl. Mech. **88**(1), 011004 (2020).
[19]F. Pan, G. Wang, L. Liu, Y. Chen, Z. Zhang, and X. Shi, "Bending induced interlayer shearing, rippling and kink buckling of multilayered graphene sheets," J. Mech. Phys. Solids **122**, 340–363 (2019).
[20]Y. Guo, J. Qiu, and W. Guo, "Mechanical and electronic coupling in few-layer graphene and hBN wrinkles: A first-principles study," Nanotechnology **27**(50), 505702 (2016).
[21]S. Xiong and G. Cao, "Bending response of single layer $MoS_2$," Nanotechnology **27**(10), 105701 (2016).
[22]J.-W. Jiang, Z. Qi, H. S. Park, and T. Rabczuk, "Elastic bending modulus of single-layer molybdenum disulfide ($MoS_2$): Finite thickness effect," Nanotechnology **24**(43), 435705 (2013).
[23]J. Yu, E. Han, M. A. Hossain, K. Watanabe, T. Taniguchi, E. Ertekin, A. M. van der Zande, and P. Y. Huang, "Designing the bending stiffness of 2D material heterostructures," Adv. Mater. **33**(9), 2007269 (2021).
[24]J. Zhao, Q. Deng, T. H. Ly, G. H. Han, G. Sandeep, and M. H. Rümmeli, "Two-dimensional membrane as elastic shell with proof on the folds revealed by three-dimensional atomic mapping," Nat. Commun. **6**(1), 8935 (2015).
[25]M. Timpel, G. Ligorio, A. Ghiami, L. Gavioli, E. Cavaliere, A. Chiappini, F. Rossi, L. Pasquali, F. Gärisch, E. J. W. List-Kratochvil, P. Nozar, A. Quaranta, R. Verucchi, and M. V. Nardi, "2D-$MoS_2$ goes 3D: Transferring optoelectronic properties of 2D $MoS_2$ to a large-area thin film," npj 2D Mater. Appl. **5**(1), 64 (2021).
[26]A. Castellanos-Gomez, M. Poot, G. A. Steele, H. S. J. van der Zant, N. Agraït, and G. Rubio-Bollinger, "Elastic properties of freely suspended $MoS_2$ nanosheets," Adv. Mater. **24**(6), 772–775 (2012).
[27]R. F. Frindt, "Single crystals of $MoS_2$ several molecular layers thick," J. Appl. Phys. **37**(4), 1928–1929 (1966).
[28]C. Casiraghi, A. Hartschuh, E. Lidorikis, H. Qian, H. Harutyunyan, T. Gokus, K. S. Novoselov, and A. C. Ferrari, "Rayleigh imaging of graphene and graphene layers," Nano Lett. **7**(9), 2711–2717 (2007).
[29]P. Nemes-Incze, Z. Osváth, K. Kamarás, and L. P. Biró, "Anomalies in thickness measurements of graphene and few layer graphite crystals by tapping mode atomic force microscopy," Carbon **46**(11), 1435–1442 (2008).
[30]X. Meng, M. Li, Z. Kang, X. Zhang, and J. Xiao, "Mechanics of self-folding of single-layer graphene," J. Phys. D **46**(5), 055308 (2013).

[31]Z. Fang, X. Li, W. Shi, Z. Li, Y. Guo, Q. Chen, L. Peng, and X. Wei, "Interlayer binding energy of hexagonal $MoS_2$ as determined by an *in situ* peeling-to-fracture method," J. Phys. Chem. C **124**(42), 23419–23425 (2020).
[32]S. Deng, E. Gao, Z. Xu, and V. Berry, "Adhesion energy of $MoS_2$ thin films on silicon-based substrates determined via the attributes of a single $MoS_2$ wrinkle," ACS Appl. Mater. Interfaces **9**(8), 7812–7818 (2017).
[33]S. Deng and V. Berry, "Wrinkled, rippled and crumpled graphene: An overview of formation mechanism, electronic properties, and applications," Mater. Today **19**(4), 197–212 (2016).
[34]P. Ares, Y. B. Wang, C. R. Woods, J. Dougherty, L. Fumagalli, F. Guinea, B. Davidovitch, and K. S. Novoselov, "Van der Waals interaction affects wrinkle formation in two-dimensional materials," Proc. Natl. Acad. Sci. U. S. A. **118**(14), e2025870118 (2021).
[35]M. M. M. Alyobi, C. J. Barnett, P. Rees, and R. J. Cobley, "Modifying the electrical properties of graphene by reversible point-ripple formation," Carbon **143**, 762–768 (2019).
[36]A. P. John, A. Thenapparambil, and M. Thalakulam, "Strain-engineering the Schottky barrier and electrical transport on $MoS_2$," Nanotechnology **31**(27), 275703 (2020).
[37]O. F. P. dos Santos and S. Azevedo, "Effect of strain on the mechanical and electronic properties of h-BN nanoribbons with 558 linear defect," Physica E **116**, 113771 (2020).